

# Yield estimation of neutron-rich rare isotopes induced by 200 MeV/u $^{132}\text{Sn}$ beams by using GEANT4

Jae Won Shin

*Department of Physics, Sungkyunkwan University, Suwon 440-746, Korea*

Kyung Joo Min

*Department of Energy Science, Sungkyunkwan University, Suwon 440-746, Korea*

Cheolmin Ham

*Department of Energy Science, Sungkyunkwan University, Suwon 440-746, Korea*

Tae-Sun Park

*Department of Physics, Sungkyunkwan University, Suwon 440-746, Korea*

Seung-Woo Hong

*Department of Physics, Sungkyunkwan University, Suwon 440-746, Korea*

---

## Abstract

A so-called “two-step reaction scheme”, in which neutron-rich rare isotopes obtained from ISOL are post-accelerated and bombarded on a second target, is employed to estimate the production yields of exotic rare isotopes. The production yields of neutron-rich rare isotope fragments induced by 200 MeV/u  $^{132}\text{Sn}$  beams bombarded on a  $^9\text{Be}$  target are estimated with Monte Carlo code, GEANT4. To substantiate the use of GEANT4 for this study, benchmark calculations are done for 80 MeV/u  $^{59}\text{Co}$ , 95 MeV/u  $^{72}\text{Zn}$ , 500 MeV/u  $^{92}\text{Mo}$ , and 950 MeV/u  $^{132}\text{Sn}$  beams on the  $^9\text{Be}$  target. It is found that  $^{132}\text{Sn}$  beams can produce neutron-rich rare isotopes with  $45 \leq Z \leq 50$

---

*Email addresses:* shine8199@skku.edu (Jae Won Shin), swhong@skku.ac.kr (Seung-Woo Hong)

more effectively than  $^{238}\text{U}$  beams at the same energy per nucleon.

*Keywords:* two-step reaction scheme, neutron-rich rare isotope, ISOL,  $^{132}\text{Sn}$  beams, GEANT4

*PACS:* 25.60.-t, 25.70.Mn, 83.10.Rs, 24.10.Lx

---

## 1. Introduction

The rare isotope beams (RIBs) provide us with immense opportunities in wide areas that are not covered by stable ion beams, which include studies of super-heavy nuclei, neutron skins, explosive nucleosynthesis and nuclear structure for neutron-rich RIs. These studies are also closely related to questions such as the origin of elements and the fundamental symmetries. By producing more exotic rare isotopes, we may approach new regions of nuclear structure and can have a chance to reach the limits of nuclear stability and previously unexplored state of matter. Productions of exotic RIBs are being carried out in facilities such as ISOLDE at CERN, ISAC at TRIUMF, RIBF at RIKEN, HRIBF at ORNL and IGISOL at JYFL, and are being planned in FRIB at MSU, SPIRAL2 at GANIL, FAIR at GSI, and SPES at INFN. The science goals to be explored with RIBs are well discussed in many reports such as U.S. Long Range Plans [1], OECD Global Science Forum [2], NuPECC Long Range Plan 2010 [3] and reviews such as Ref. [4].

Some of the facilities mentioned above use Isotope Separation On Line (ISOL) method [5, 6] to produce RIBs, while others use In-Flight Fragmentation (IFF) method [7, 8]. However, as an attempt for producing extremely neutron-rich isotopes, a so-called “two-step reaction scheme” (TSRS) has been suggested in Ref. [9]. By post-accelerating some of the fission fragments from ISOL and fragmenting them one step further, one could produce even more neutron-rich nuclei covering a wider region of elements which would be

poorly populated by using only either ISOL or IFF method. It was suggested that a long-lived neutron-rich rare isotope such as  $^{132}\text{Sn}$  produced by fission of  $^{238}\text{U}$  induced by proton beams could be a good candidate as primary RIBs.

Recently, TSRS has been experimentally validated at the FRagment Separator (FRS) in GSI [10], where they have first produced  $\sim 10^3$   $^{132}\text{Sn}$   $\text{s}^{-1}$  by impinging 950 MeV/u  $^{238}\text{U}$  beams on the Pb target and bombarded  $^{132}\text{Sn}$  beams on a  $^9\text{Be}$  target. Their results indicate that TSRS can be indeed effective in producing more exotic medium-mass neutron-rich isotopes. According to the design summary of RAON in Korea [11, 12, 13], the expected intensity of  $^{132}\text{Sn}$  can be as large as about  $10^8$  particles per second (pps). It is the unique feature of RAON that the isotopes generated by ISOL can be post-accelerated and injected to the IFF facility for producing more exotic RIBs.

In this work, we have performed GEANT4 (GEometry ANd Tracking) [14, 15] simulations for estimating the production yields of exotic rare isotopes by using TSRS. We have calculated the yields of rare isotopes by considering the bombardment of 200 MeV/u  $^{132}\text{Sn}$  and  $^{238}\text{U}$  beams on the  $^9\text{Be}$  target and compared the results. By comparing the yields from the two different beams, we may quantify the efficiency of TSRS in producing neutron-rich rare isotopes. GEANT4 has been used for a number of simulations, but has not been used much for nucleus-nucleus (AA) collisions. For checking the validity of the use of GEANT4 for this purpose, we have first calculated the isotopic production cross sections for AA collisions and compared them with experimental data as well as with those obtained from another Monte Carlo code, PHITS [16]. We have also compared the results with the predictions from other popular empirical models, EPAX2 [17] and EPAX3 [18].

The outline of the paper is as follows. In Sec. 2, the simulation methods

used in our study are summarized. In Sec. 3, we first show benchmark calculation results and present the production yields of the isotopes obtained by  $^{132}\text{Sn}$  and  $^{238}\text{U}$  beams at 200 MeV/u. A summary is given in Sec. 4.

## 2. Simulation method

Before we use GEANT4 (v10.0) [14, 15] for TSRS, we have first performed benchmark simulations. The production cross sections of the isotopes fragmented by AA collisions are calculated by using hadronic models such as G4BinaryLightIonReaction [19, 20] and G4QMDReaction [21]. We have also performed similar simulations with PHITS (v2.52) [16] by using JAERI Quantum Molecular Dynamics (JQMD) [22] for comparison with the results from GEANT4.

We distinguish our simulation methods by referring to them as “G4-BIN”, “G4-QMD” and “P-JQMD”:

- G4-BIN: GEANT4 simulation with G4BinaryLightIonReaction model [19, 20].
- G4-QMD: GEANT4 simulation with G4QMDReaction model [21].
- P-JQMD: PHITS simulation with JAERI Quantum Molecular Dynamics (JQMD) [22].

To see the effectiveness of TSRS, the production yields of rare isotopes by bombarding 200 MeV/u  $^{132}\text{Sn}$  and  $^{238}\text{U}$  beams on the  $^9\text{Be}$  target are calculated and compared with each other. As our simulation model, the G4-BIN is used for the calculations because the model gives reliable results as will be shown in Sec. 3.1. In the production of the isotopes through the fragmentation by AA collisions, ionization processes cause the energy loss of the ions in the target. The G4ionIonisation is used for simulating such

energy losses. The above mentioned hadronic and electromagnetic models are described on the web [23], and the Physics Reference Manual [24] is also available.

### 3. Results

#### 3.1. Benchmark test of simulation methods for the production cross sections

AA collisions involve extremely complicated processes, and it is not yet well established how accurately various simulation tools can describe them. We thus begin with presenting our benchmarking calculations for the adopted hadronic models.

Recently, several simulations have been performed for AA collisions with stable beams such as  $^{12}\text{C}$  [25, 26, 27],  $^{20}\text{Ne}$  and  $^{24}\text{Mg}$  [28],  $^{40}\text{Ar}$  [29, 30], and  $^{56}\text{Fe}$  [30, 31] by using Monte Carlo codes such as GEANT4, PHITS, FLUKA [32, 33] and so on. In these studies, partial and total fragmentation cross sections have been calculated, and reasonable agreements with the experimental data are obtained.

In this work, we extend such studies by considering heavier neutron-rich beams including 80 MeV/u  $^{59}\text{Co}$  [34], 95 MeV/u  $^{72}\text{Zn}$  [35], 500 MeV/u  $^{92}\text{Mo}$  [36], and 950 MeV/u  $^{132}\text{Sn}$  [10] beams. Furthermore, in contrast to the above studies [25, 26, 27, 28, 29, 30, 31], in which the production cross sections are calculated for each element with a sum over isotopes, we analyze the ‘isotopic’ production cross sections of AA collisions for detailed comparisons.

Our calculated production cross sections for the above reactions are shown in Figs. 1 ~ 4 by the filled symbols; the red circles for G4-BIN, the blue squares for G4-QMD and the orange triangles for P-JQMD. For comparison, we have also plotted the predictions from EPAX2 [17] (the dashed lines) and EPAX3 [18] (the solid lines) together with the experimental data (the open

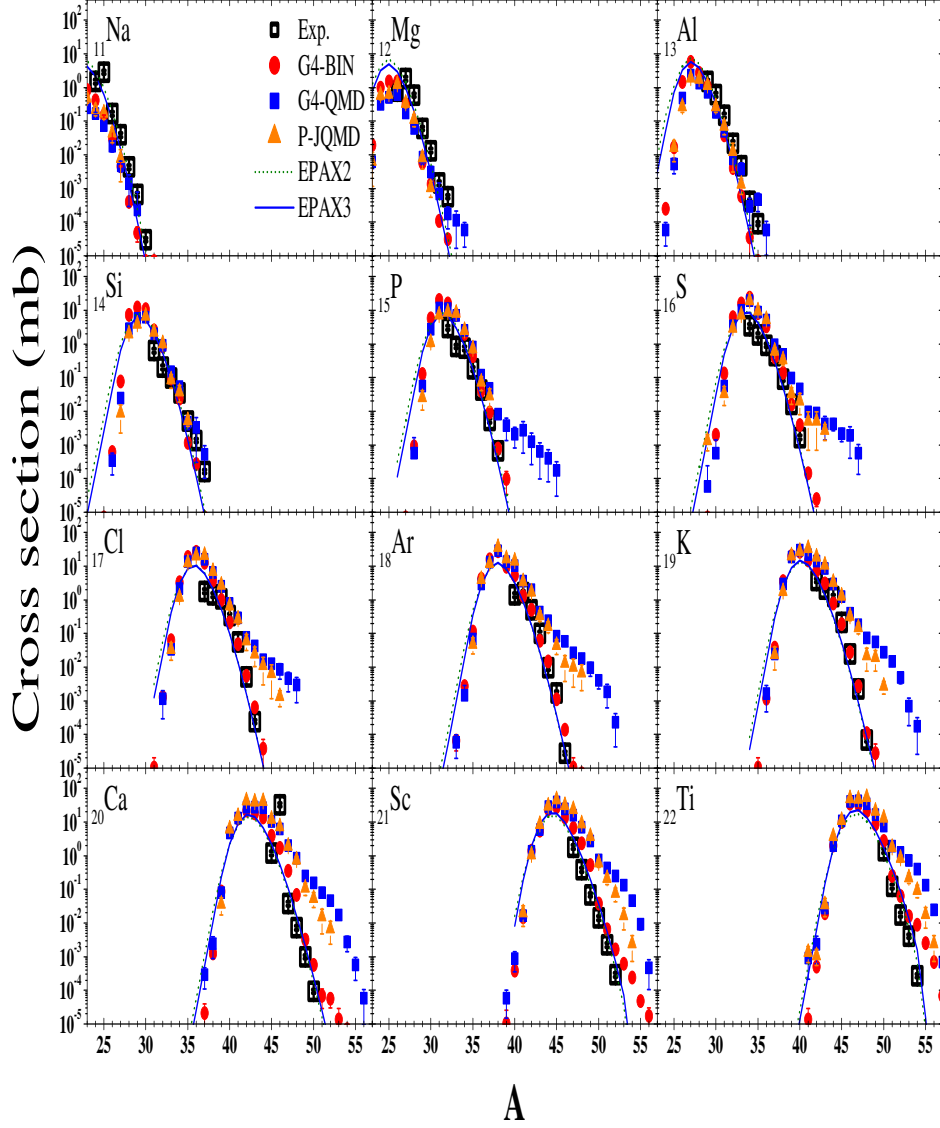


Figure 1: (Color online) Production cross sections of various isotopes due to the collision  $^{59}\text{Co} + ^9\text{Be}$  at 80 MeV/u. The open squares in black denote the experimental data [34], and the dashed (solid) lines represent EPAX2 (EPAX3) results. The simulation results are denoted by the filled symbols; the red circles for G4-BIN, the blue squares for G4-QMD and the orange triangles for P-JQMD.

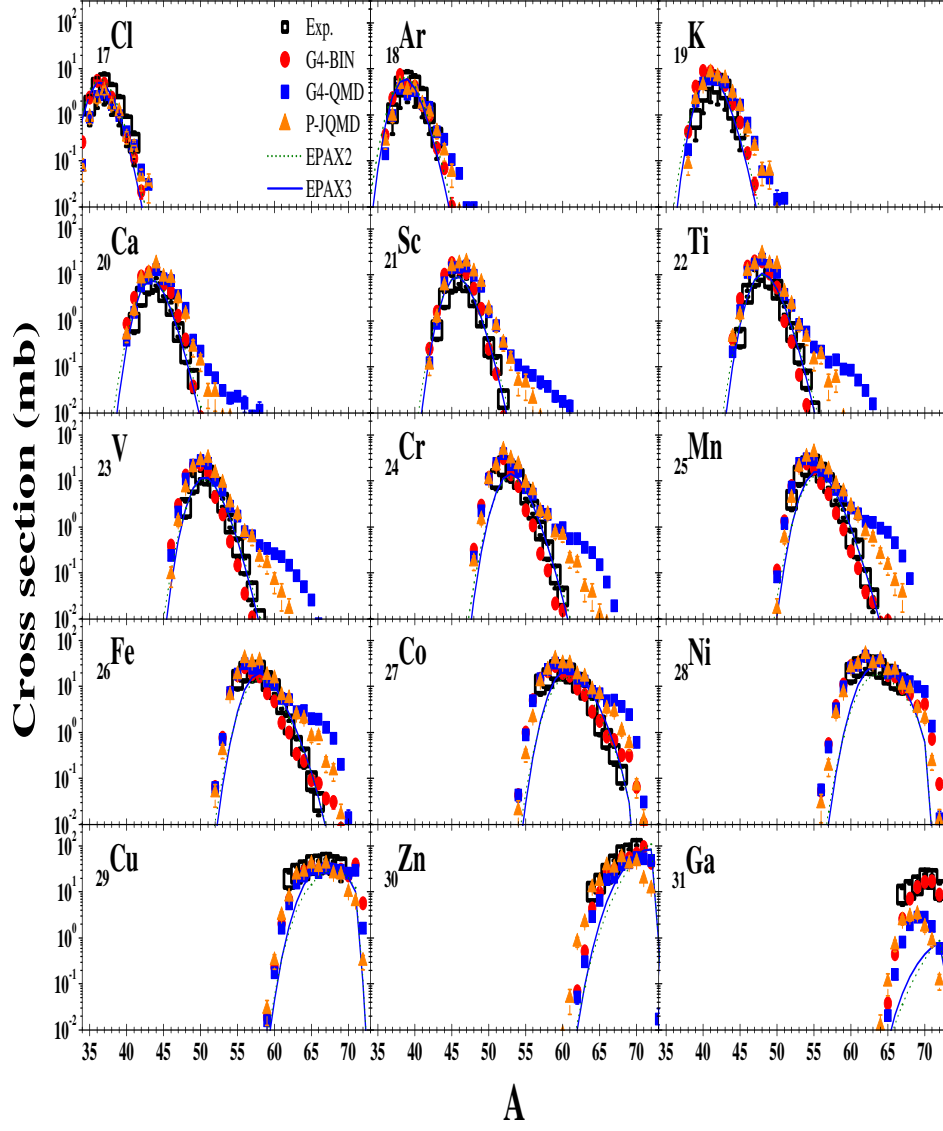


Figure 2: (Color online) Production cross sections of various isotopes due to the collision  $^{72}\text{Zn} + ^9\text{Be}$  at 95 MeV/u. The open squares in black denote the experimental data [35]. See the caption of Fig. 1 for the meaning of other symbols.

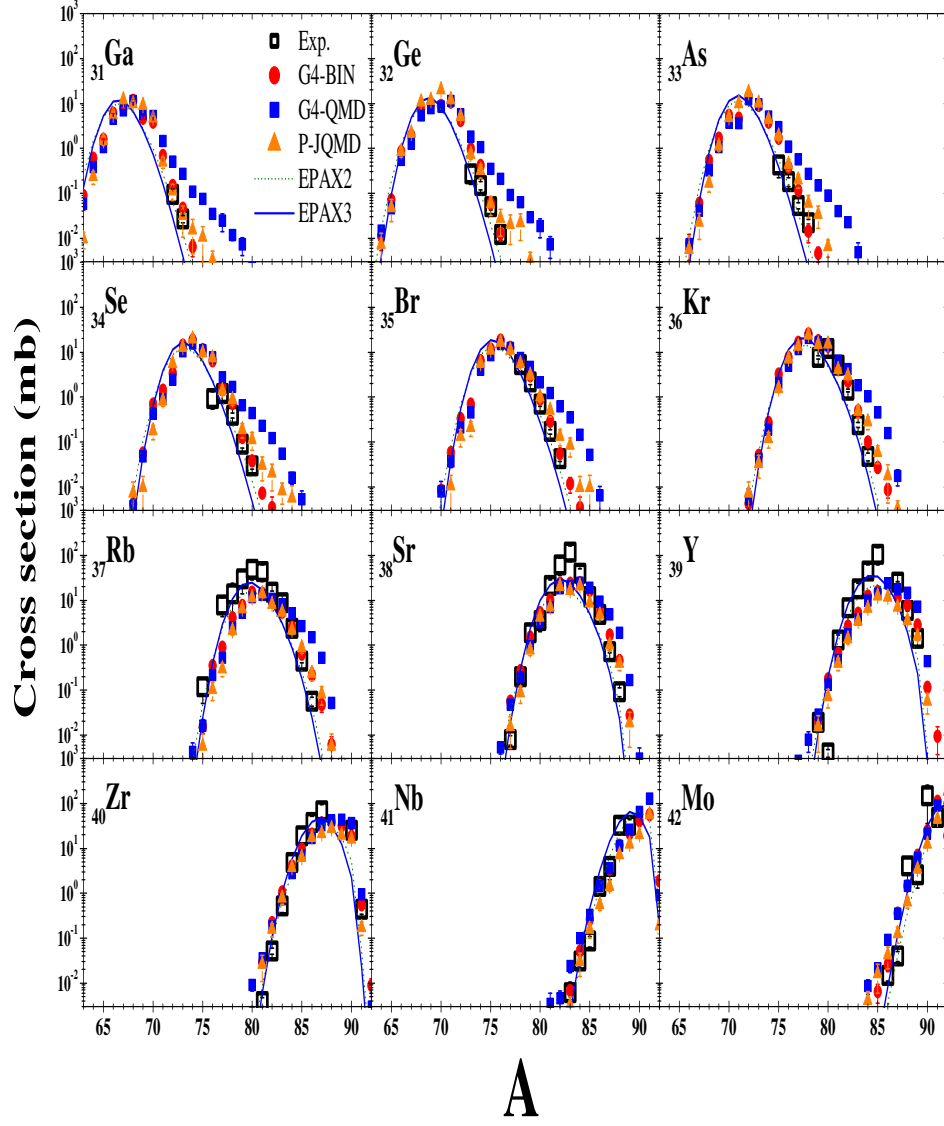


Figure 3: (Color online) Production cross sections of various isotopes due to the collision  $^{92}\text{Mo} + ^9\text{Be}$  at 500 MeV/u. The open squares in black denote the experimental data [36]. See the caption of Fig. 1 for the meaning of other symbols.



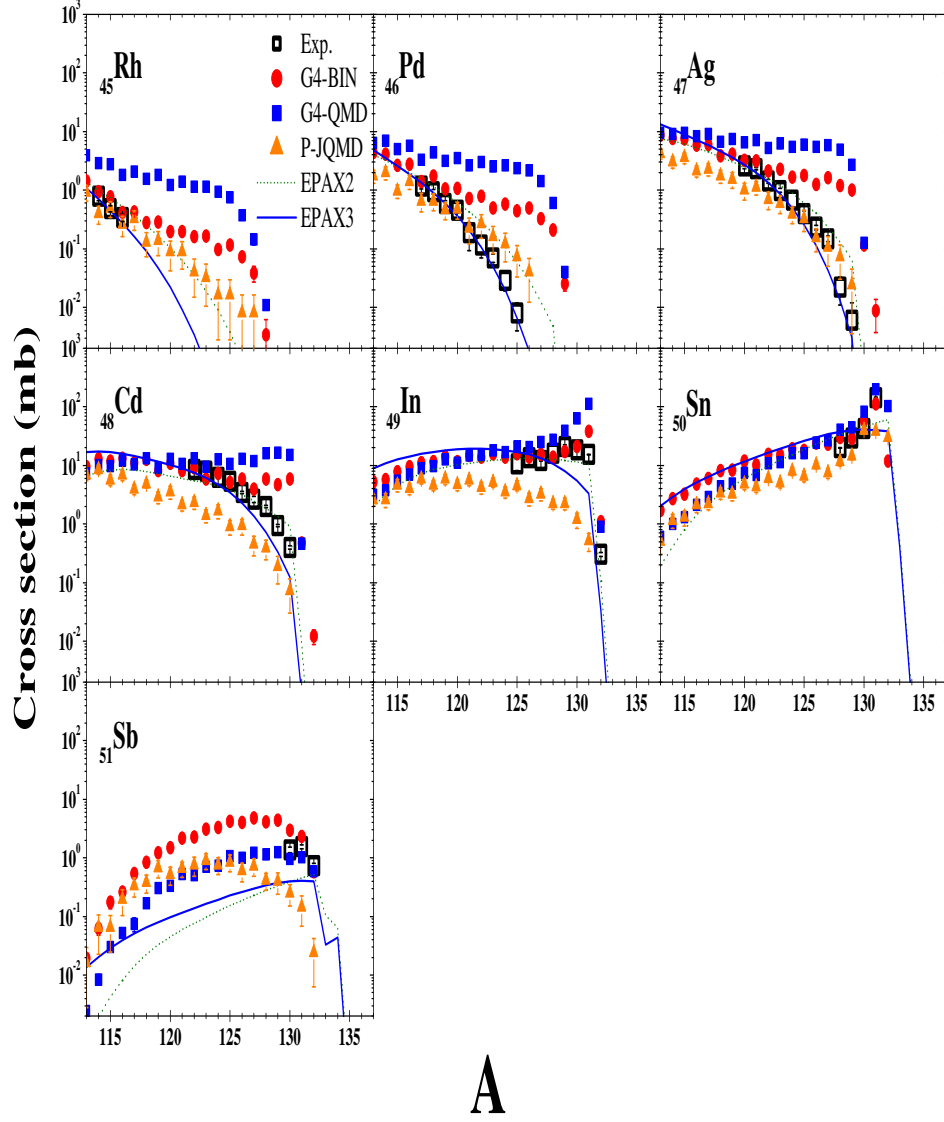


Figure 4: (Color online) Production cross sections of various isotopes due to the collision  $^{132}\text{Sn} + ^9\text{Be}$  at 950 MeV/u. The open squares in black denote the experimental data [10]. See the caption of Fig. 1 for the meaning of other symbols.

squares in black) taken from the EXFOR database [37].

Figures 1~3 show the results for 80 MeV/u  $^{59}\text{Co}$ , 95 MeV/u  $^{72}\text{Zn}$ , and 500 MeV/u  $^{92}\text{Mo}$  beams, respectively. The G4-BIN (red circles) is found to be superior to other models in reproducing the experimental data. EPAX2 and EPAX3 also reproduce well the experimental data for most cases, but underestimate in some cases, in particular, for the production of the  $_{31}\text{Ga}$  isotopes for  $^{72}\text{Zn}$  beams. P-JQMD (orange triangles) and G4-QMD (blue squares) overestimate the production of neutron-rich isotopes of heavier elements by a factor of  $\lesssim 10^4$ , while their results for light elements are as good as those from G4-BIN.

In Fig. 4, the results for  $^{132}\text{Sn} + ^9\text{Be}$  reactions at 950 MeV/u are shown. None of the models can reproduce all the experimental data satisfactorily. P-JQMD underestimates the production of  $_{48}\text{Cd} \sim _{51}\text{Sb}$  isotopes, while G4-QMD overestimates the production of  $_{45}\text{Rh} \sim _{49}\text{In}$  isotopes by a factor of  $\lesssim 10^3$ . On the other hand, EPAX2 and EPAX3 show rather good overall agreements, though EPAX2 overestimates the production of  $_{46}\text{Pd}$  isotopes, EPAX3 underestimates neutron-rich isotopes of  $_{49}\text{In}$ , and both underestimate  $_{51}\text{Sb}$  isotopes. Finally, G4-BIN, which shows the best performance for other cases, is also found to overestimate the productions of  $_{46}\text{Pd}$ ,  $_{47}\text{Ag}$ , and  $_{48}\text{Cd}$  isotopes by  $\lesssim 10^2$ . Such overestimation of the production cross sections needs to be ultimately resolved by improving the hadronic models, but it is beyond the scope of this work.

These benchmark calculations show that G4-BIN gives the best results among the three models. Although the benchmark calculations are done for 950 MeV/u  $^{132}\text{Sn}$  beams, it is expected that G4-BIN would work better than other models for 200 MeV/u  $^{132}\text{Sn}$  beams as well for the following reason. In Fig. 5 we have plotted experimental production cross sections of  $_{46}\text{Pd} \sim$

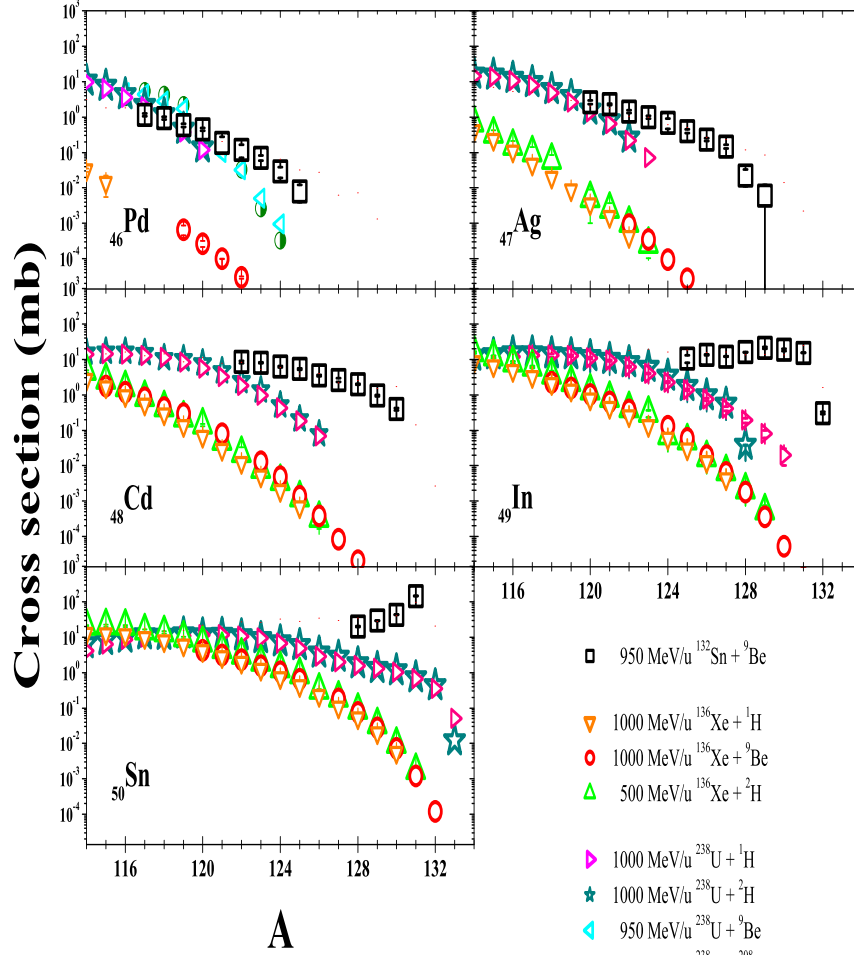


Figure 5: (Color online) The experimental production cross sections of  $^{46}\text{Pd} \sim ^{50}\text{Sn}$  isotopes. The black boxes represent the production cross sections from 950 MeV/u  $^{132}\text{Sn} + {}^9\text{Be}$  [10]. The orange inverted triangles are those from 1000 MeV/u  $^{136}\text{Xe} + {}^1\text{H}$  [38], the red circles from 1000 MeV/u  $^{136}\text{Xe} + {}^9\text{Be}$  [39], and the green triangles from 500 MeV/u  $^{136}\text{Xe} + {}^2\text{H}$  [40]. The pink triangles are from 1000 MeV/u  $^{238}\text{U} + {}^1\text{H}$  [41], the blue stars from 1000 MeV/u  $^{238}\text{U} + {}^2\text{H}$  [42], the blue triangles from 950 MeV/u  $^{238}\text{U} + {}^9\text{Be}$  [43], and the green circles from 950 MeV/u  $^{238}\text{U} + {}^{208}\text{Pb}$  [43].

$_{50}\text{Sn}$  isotopes for  $^{132}\text{Sn}$  [10],  $^{136}\text{Xe}$  [40, 38, 39] and  $^{238}\text{U}$  [41, 42, 43] beams. The experimental cross sections are nearly independent of the incident beam energies [18, 26, 35, 44, 45, 46, 47, 40]. It is clearly seen that the cross sections are mainly characterized by the species of the incident beams, and the energy-dependence is rather weak.

We plot in Fig. 6 G4-BIN predictions for the production cross sections of  $_{45}\text{Rh} \sim _{50}\text{Sn}$  isotopes due to the  $^{132}\text{Sn}$  beams at 100, 200, 300, 500 and 950 MeV/u. The G4-BIN predictions at the energy of  $\sim 200$  MeV/u agree well with the 950 MeV/u data regardless of the atomic number  $Z$ . If the aforementioned experimentally observed energy-independence of the cross section still holds down to 200 MeV/u, we expect a good agreement will be obtained between the data and the G4-BIN predictions at 200 MeV/u, for which the beam energy is being planned for RAON [11, 12, 13]. In fact, G4-BIN shows a small energy-dependence. While the calculated yields induced by 200 MeV/u  $^{132}\text{Sn}$  beams agree with the experimental data obtained at 950 MeV/u, G4-BIN prediction made at 950 MeV/u overestimates the data obtained at 950 MeV/u for  $_{46}\text{Pd}$ ,  $_{47}\text{Ag}$ , and  $_{48}\text{Cd}$  isotopes with larger  $A$ . The energy-dependence of the G4-BIN is weak for  $Z=49$  and  $50$ , but becomes noticeable as  $Z$  decreases below 49.

Similar features can be seen for  $^{136}\text{Xe}$  beams, whose experimental data are available at 500 and 1000 MeV/u. As shown in Fig. 7, the experimental data are rather independent of energy. The predicted cross sections at 200 MeV/u are close to the data obtained at 500 and 1000 MeV/u, and the calculated cross sections show some energy dependence for isotopes with larger  $A$ , which is a feature observed for  $^{132}\text{Sn}$  beams as well.

From the above comparisons of the results by using different models, it is found that the G4-BIN gives most reasonable results for the isotopic

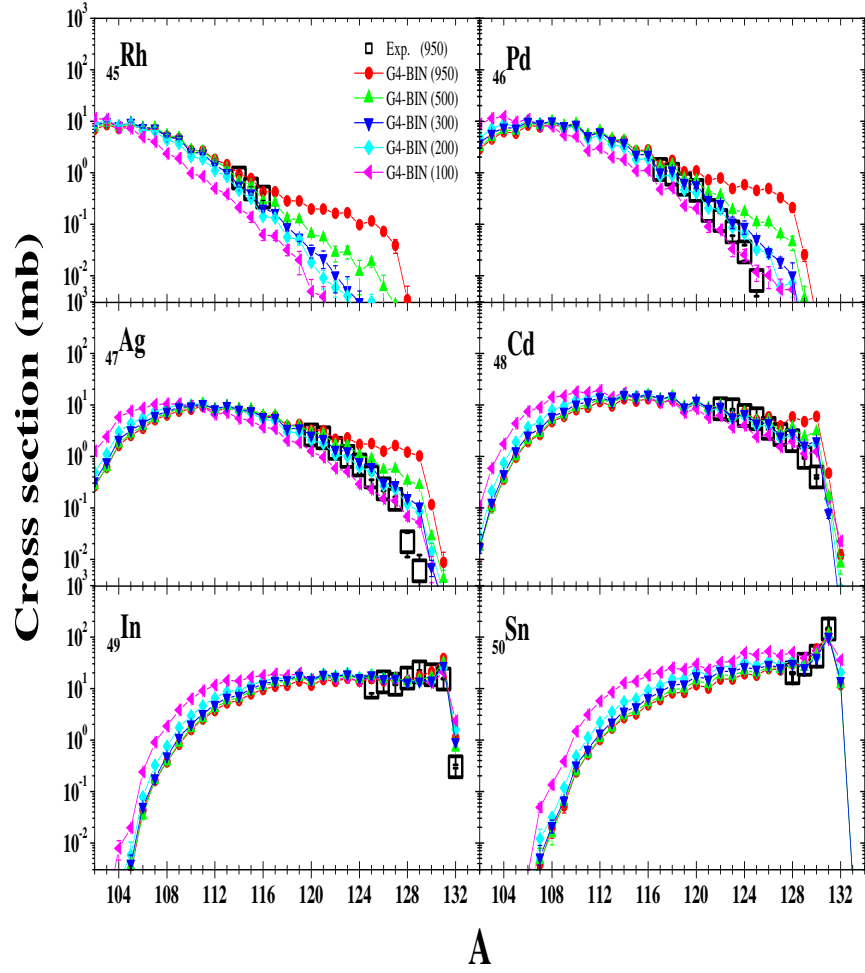


Figure 6: (Color online) Production cross sections of  $^{132}\text{Sn} + ^9\text{Be}$ . The open squares in black denote the experimental data at 950 MeV/u [10], and the filled symbols with lines represent the G4-BIN results for a few selected incident energies.

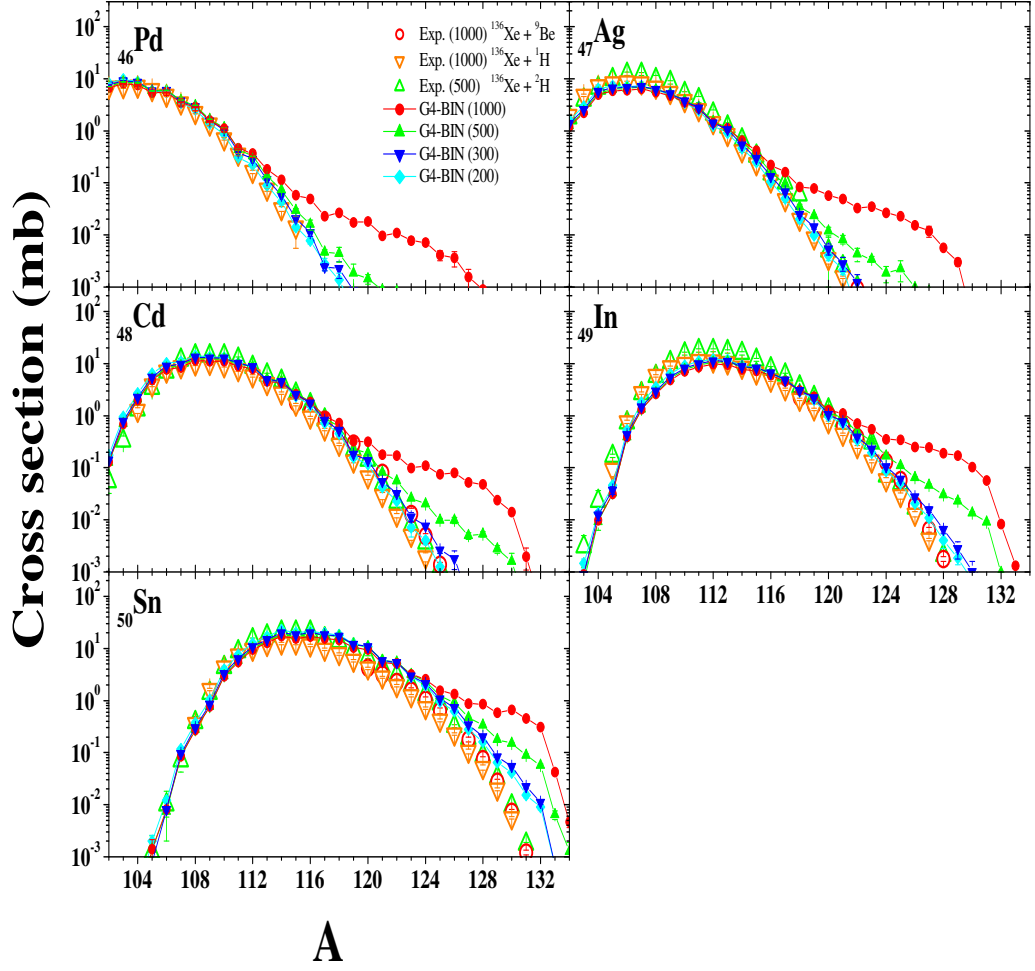


Figure 7: (Color online) Production cross sections of  $^{136}\text{Xe}$  beams. The red circles are for 1000 MeV/u  $^{136}\text{Xe} + ^9\text{Be}$  [39], the inverted orange triangles are for 1000 MeV/u  $^{136}\text{Xe} + ^1\text{H}$  [38], and the green triangles for 500 MeV/u  $^{136}\text{Xe} + ^2\text{H}$  [40]. The filled symbols with lines denote the G4-BIN results for a few selected values of incident energy.

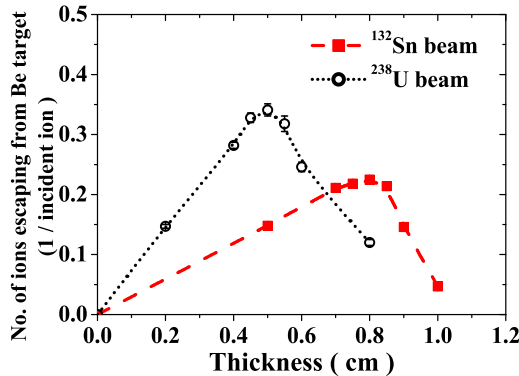


Figure 8: (Color online) The total number of ions per incident ion escaping from the Be target. The red squares and the open black circles denote the results from  $^{132}\text{Sn}$  and  $^{238}\text{U}$  beams of 200 MeV/u, respectively. The dotted and the dashed lines are to guide the eyes.

productions among the three models. The G4-QMD does not reproduce well the experimental data especially for the production of neutron-rich isotopes. The P-JQMD either overestimates or underestimates the experimental data. Thus, we have chosen the G4-BIN as our simulation model, and the results presented in the next subsection are calculated by the G4-BIN.

### 3.2. Production yields of neutron rich isotopes by using TSRS

To see the effectiveness of TSRS, one needs to estimate the production yields from TSRS. Production yields are sensitive to the target thickness. As the target thickness increases, the number of the collisions between the incident ions and the target nuclei also increases. But if the target is too thick, it becomes hard for the generated nuclides to escape from the target. Figure 8 shows the dependence of the yields on the target thicknesses. It can be seen that at the energy of 200 MeV/u the optimal thickness is 0.8 cm and 0.5 cm for  $^{132}\text{Sn}$  and  $^{238}\text{U}$  beams, respectively, and thus these thicknesses are chosen for our simulations of the production yields.

A schematic geometrical setup of our simulation is depicted in Fig. 9.

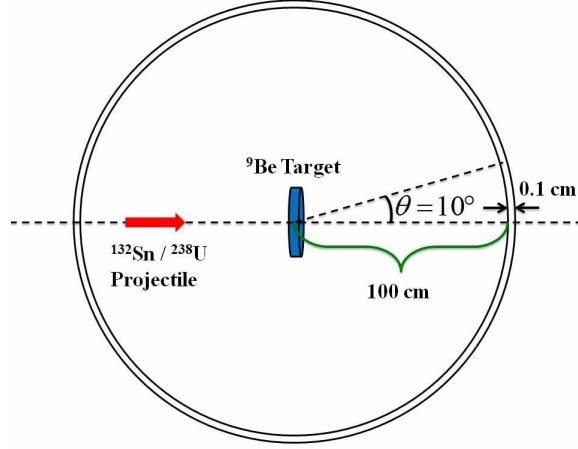


Figure 9: Schematic diagram of the simulation setup.

Incident ions are treated as a pencil beam. The  ${}^9\text{Be}$  target is modeled as a cylinder of radius 1 cm, whose thickness is chosen as 0.8 cm and 0.5 cm for  ${}^{132}\text{Sn}$  and  ${}^{238}\text{U}$  beams, respectively. The scoring region of a spherical shell shape is placed surrounding the target. The inner and the outer radii of the scoring region are chosen to be 100 cm and 100.1 cm, respectively. The target area is in vacuum, and the thickness of the scoring region is chosen as 0.1 cm arbitrarily for convenience and does not affect the results. We score only those isotopes that reach the scoring region. The scoring shell consists of 18 angular bins with an interval of 10 degrees. We find that about  $\sim 98\%$  of the yields are concentrated in the forward direction with  $\theta < 10^\circ$  and thus we show only the scoring results in the bin with  $\theta < 10^\circ$  for convenience.

Figure 10 shows the yields of the nuclides produced by 200 MeV/u  ${}^{132}\text{Sn}$  and  ${}^{238}\text{U}$  beams.  ${}^{132}\text{Sn}$  beams produce isotopes mainly with  $45 \leq Z \leq 50$ , while the products induced by  ${}^{238}\text{U}$  beams are concentrated in the diagonal region of the N-Z plane that mainly consists of stable nuclides. We plot the ratios of the yields of the nuclides produced by  ${}^{132}\text{Sn}$  to those produced by  ${}^{238}\text{U}$  in Fig. 11, which clearly shows that  ${}^{132}\text{Sn}$  can produce more neutron-



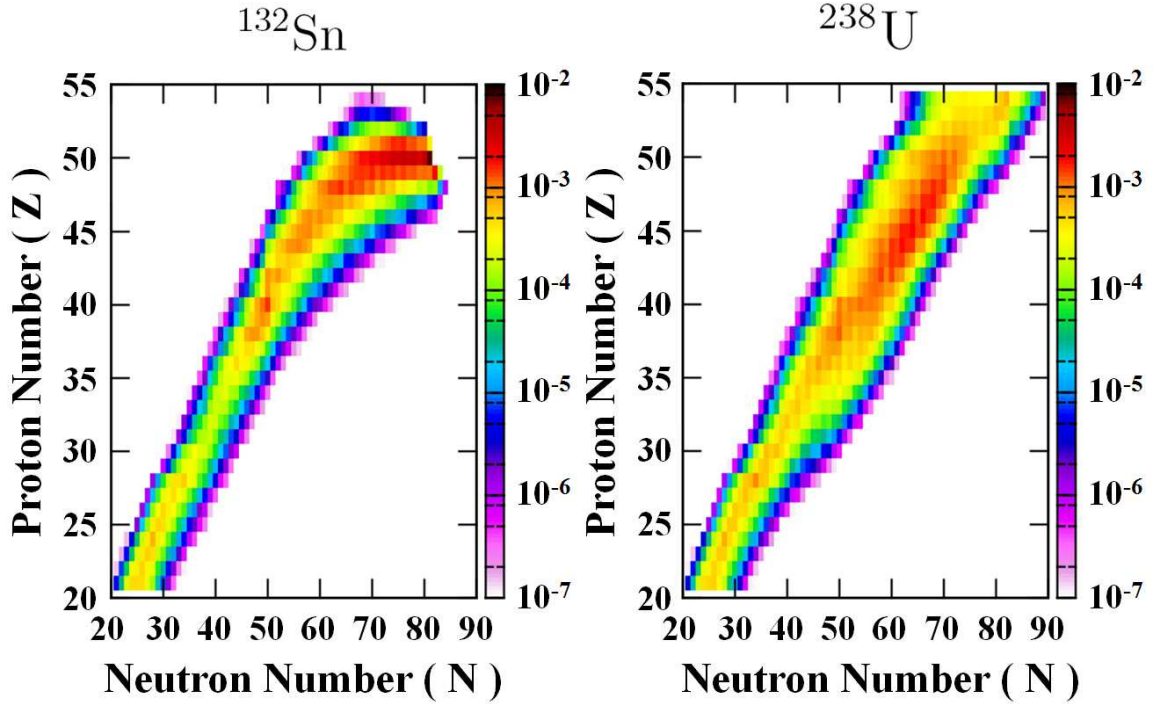


Figure 10: (Color online) The isotopic production yields plotted in the N-Z plane, for 200 MeV/u  $^{132}\text{Sn}$  (left) and  $^{238}\text{U}$  (right) beams on the  $^9\text{Be}$  target.

rich isotopes of  $45 \leq Z \leq 50$  by nearly two or three orders of magnitudes than  $^{238}\text{U}$  beams.

Detailed production yields of nuclides are shown in Fig. 12, where the yields of  $_{45}\text{Rh} \sim _{50}\text{Sn}$  isotopes due to  $^{132}\text{Sn}$  and  $^{238}\text{U}$  beams are plotted with respect to the mass number  $A$ . The yield curves due to  $^{238}\text{U}$  beams are more or less parabolic, having the maximum yield value ( $\sim 10^{-3}$  per incident ion) at around  $A \simeq 2 \times Z + 20$  for all the  $Z$  values considered here. As  $Z$  increases, the curves shift to the region of higher  $A$ , but their shapes are almost unchanged for different elements. This behavior is in accordance with the right panel of Fig. 10, which shows that the population of the fission fragments of  $^{238}\text{U}$  is concentrated in the diagonal region in the N-Z plane.

The yield curves due to  $^{132}\text{Sn}$  beams also show the tendency to shift to

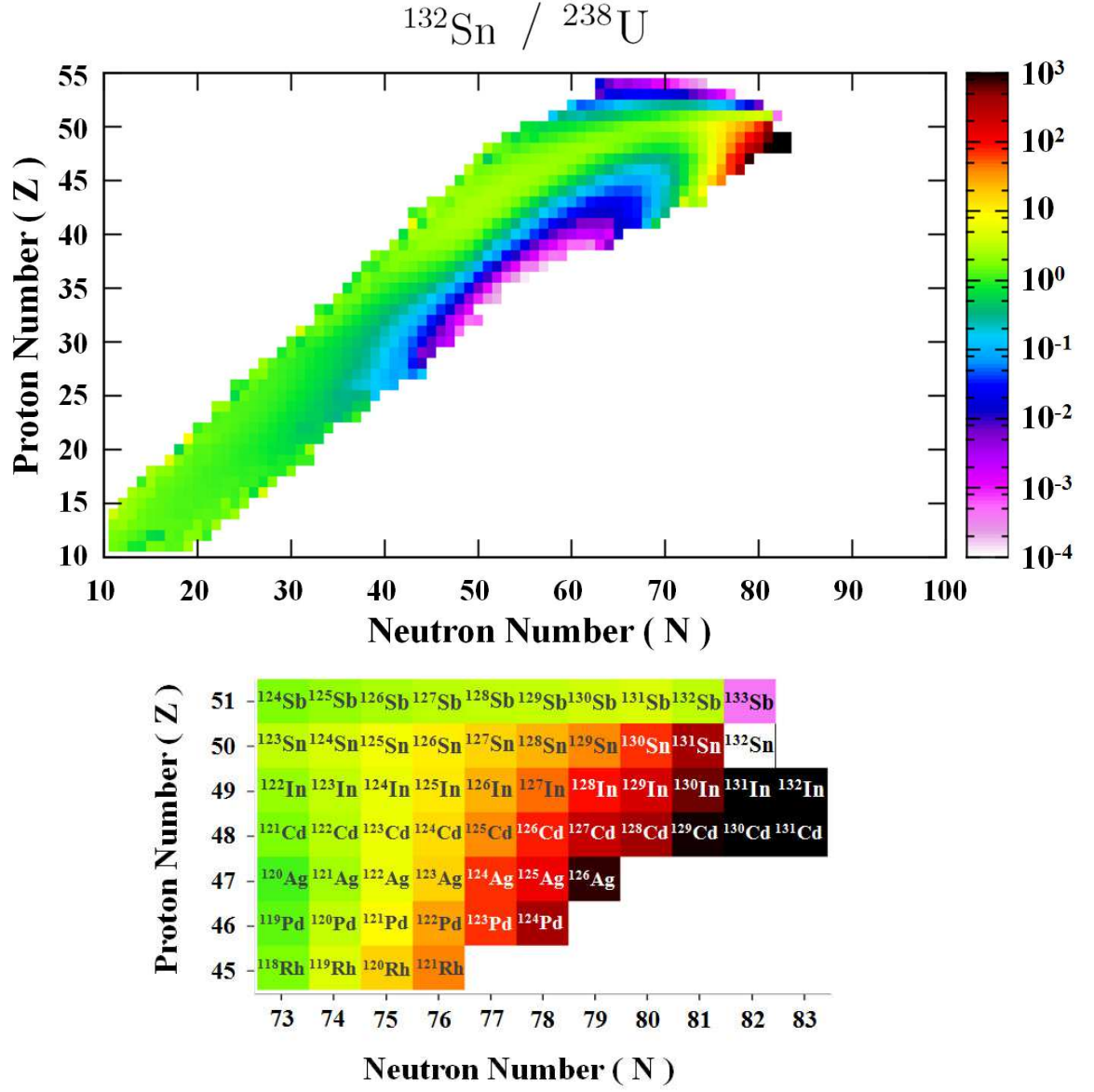


Figure 11: (Color online) The ratios of the yields due to  $^{132}\text{Sn}$  beams to the yields due to  $^{238}\text{U}$  beams. The region where the ratio is greater than  $10^3$  is denoted by black.

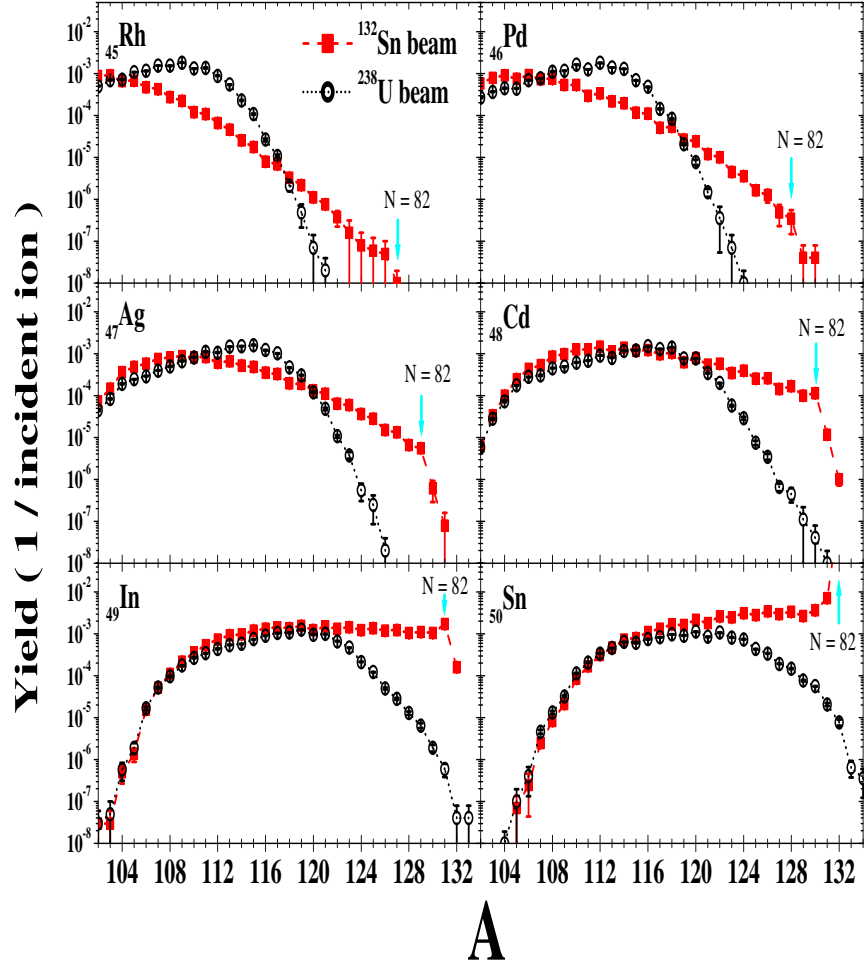


Figure 12: (Color online) Yields of  $^{45}\text{Rh} \sim ^{50}\text{Sn}$  isotopes with respect to mass number  $A$ . The red squares and the open black circles denote the yields induced by  $^{132}\text{Sn}$  and  $^{238}\text{U}$  beams, respectively.

higher  $A$  values as  $Z$  increases, and are similar to those of  $^{238}\text{U}$  in the light mass region for most elements. But the curves deviate from those of  $^{238}\text{U}$  in the heavier mass region. The tails of the yield curves for  $^{132}\text{Sn}$  beams in the larger  $A$  region do not drop as rapidly as those for  $^{238}\text{U}$ . This shows that  $^{132}\text{Sn}$  can produce more effectively neutron-rich isotopes than  $^{238}\text{U}$  beams. This tendency becomes stronger as  $Z$  increases, and the tail for  $_{49}\text{In}$  becomes almost flat up to  $N=82$ . The mass region where the yields due to  $^{132}\text{Sn}$  exceed those of  $^{238}\text{U}$  keeps increasing in general with higher  $Z$ :  $A \geq 118$  for  $_{45}\text{Rh}$ ,  $A \geq 119$  for  $_{46}\text{Pd}$ ,  $A \geq 120$  for  $_{47}\text{Ag}$ ,  $A \geq 122$  for  $_{48}\text{Cd}$ ,  $A \geq 123$  for  $_{49}\text{In}$ , and  $A \geq 114$  for  $_{50}\text{Sn}$ .

Note that the yield curves due to  $^{132}\text{Sn}$  beams show a shell structure with the cusps developed at the magic number  $N=82$ . The yield for  $N=82$  isotope is about  $10^{-8}$  for  $_{45}^{127}\text{Rh}$ ,  $10^{-6}$  for  $_{46}^{128}\text{Pd}$ ,  $10^{-5}$  for  $_{47}^{129}\text{Ag}$ ,  $10^{-4}$  for  $_{48}^{130}\text{Cd}$  and  $2 \times 10^{-3}$  for  $_{49}^{131}\text{In}$  in the unit of  $1/(\text{incident ion})$ . For all the cases considered, the yields for the isotopes with  $N > 82$ , which means more neutrons than the incident  $^{132}\text{Sn}$  beams, are found to be suppressed by a factor of  $\simeq 10$  for each additional neutron.

Our results show that at the energy of 200 MeV/u  $^{132}\text{Sn}$  beams is more effective than  $^{238}\text{U}$  beams in producing neutron-rich isotopes. In particular, the yields are enhanced by factors of  $10^3$  for  $^{131,132}\text{In}$ ,  $^{129,130,131}\text{Cd}$  and  $^{127}\text{Ag}$ .

#### 4. Summary

We have conducted a simulation study for the isotope production yields induced by 200 MeV/u  $^{132}\text{Sn}$  and  $^{238}\text{U}$  beams on the  $^9\text{Be}$  target by using G4BinaryLightIonReaction (G4-BIN) hadronic model provided by GEANT4 as our main engine after considering three simulation methods such as G4-BIN, G4-QMD and P-JQMD. For the production of neutron-rich isotopes

with  $45 \leq Z \leq 50$ ,  $^{132}\text{Sn}$  is found to be much more efficient than  $^{238}\text{U}$  beams, supporting the usefulness of the TSRS mechanism.

In our benchmark calculations for the production cross sections to check the accuracy of hadronic models, however, we have observed that the G4-BIN has overestimated the production of neutron-rich isotopes for  $_{46}\text{Pd}$ ,  $_{47}\text{Ag}$ , and  $_{48}\text{Cd}$  isotopes with 950 MeV/u  $^{132}\text{Sn}$  beams. As discussed in Sec. 3.1, the experimental production cross sections of  $_{46}\text{Pd} \sim _{50}\text{Sn}$  isotopes induced by  $^{132}\text{Sn}$  [10],  $^{136}\text{Xe}$  [40, 38, 39] and  $^{238}\text{U}$  [41, 42, 43] beams are quite energy-independent, while the calculated production cross sections have some energy dependence. Thus, our simulation results with 200 MeV/u beams is expected to have some uncertainty, though it seems small and remains to be resolved.

## Acknowledgement

This work was supported in part by the Basic Science Research Program through the Korea Research Foundation (NRF-2013R1A1A2063824, NRF-2012R1A1A2007826, NRF-2012M2B2A4030183).

## References

- [1] The DOE/NSF Nuclear Science Advisory Committee, Opportunities in Nuclear Science—A Long-Range Plan for the Next Decade, Available online at [http://science.energy.gov/~media/np/nsac/pdf/docs/lrp\\_5547\\_final.pdf](http://science.energy.gov/~media/np/nsac/pdf/docs/lrp_5547_final.pdf) (April 2002).
- [2] OECD, Report of the Working Group on Nuclear Physics, Available online at <http://www.oecd.org/sti/sci-tech/40638321.pdf> (May 2008).

- [3] The European Science Foundation, NuPECC Long Range Plan 2010: Perspectives of Nuclear Physics in Europe, Available online at [http://www.nupecc.org/pub/lrp10/lrp2010\\_final\\_hires.pdf](http://www.nupecc.org/pub/lrp10/lrp2010_final_hires.pdf) (November 2010).
- [4] D. F. Geesaman, C. K. Gelbke, R. V. F. Janssens, B. M. Sherrill, PHYSICS OF A RARE ISOTOPE ACCELERATOR, *Annu. Rev. Nucl. Part. Sci.* 56 (2006) 53–92. doi:10.1146/annurev.nucl.55.090704.151604.
- [5] O. Kofoed-Hansen, K. O. Nielsen, Short-Lived Krypton Isotopes and Their Daughter Substances, *Phys. Rev.* 82 (1951) 96–97. doi:10.1103/PhysRev.82.96.2.
- [6] O. Kofoed-Hansen, K. O. Nielsen, Measurements on shortlived radioactive krypton isotopes from fission after isotopic separation, Vol. 26, I kommission hos Munksgaard, 1951.
- [7] I. Tanihata, H. Hamagaki, O. Hashimoto, S. Nagamiya, Y. Shida, N. Yoshikawa, O. Yamakawa, K. Sugimoto, T. Kobayashi, D. E. Greiner, N. Takahashi, Y. Nojiri, Measurements of interaction cross sections and radii of He isotopes, *Phys. Lett. B* 160 (1985) 380–384. doi:10.1016/0370-2693(85)90005-X.
- [8] I. Tanihata, H. Hamagaki, O. Hashimoto, Y. Shida, N. Yoshikawa, K. Sugimoto, O. Yamakawa, T. Kobayashi, Measurements of Interaction Cross Sections and Nuclear Radii in the Light p-Shell Region, *Phys. Rev. Lett.* 55 (1985) 2676–2679. doi:10.1103/PhysRevLett.55.2676.
- [9] K. Helariutta, J. Benlliure, M. V. Ricciardi, K.-H. Schmidt, Model calculations of a two-step reaction scheme for the production of

- neutron-rich secondary beams, *Eur. Phys. J. A* 17 (2003) 181–193.  
doi:10.1140/epja/i2003-10005-7.
- [10] D. Pérez-Loureiro, et al., Production of neutron-rich nuclei in fragmentation reactions of  $^{132}\text{Sn}$  projectiles at relativistic energies, *Phys. Lett. B* 703 (2011) 552–556. doi:10.1016/j.physletb.2011.08.037.
- [11] Rare Isotope Science Project, Baseline Design Summary, Available online at [http://www.ibs.re.kr/eng/sub02\\_08.do](http://www.ibs.re.kr/eng/sub02_08.do) (August 2012).
- [12] J. K. Ahn, et al., Overview of the KoRIA Facility for Rare Isotope Beams, *Few-Body Syst.* 54 (2013) 197–204. doi:10.1007/s00601-012-0359-5.
- [13] Y. K. Kwon, et al., Status of Rare Isotope Science Project in Korea, *Few-Body Syst.* 54 (2013) 961–966. doi:10.1007/s00601-013-0605-5.
- [14] S. Agostinelli, et al., GEANT4—a simulation toolkit, *Nucl. Instrum. Meth. A* 506 (2003) 250–303. doi:10.1016/S0168-9002(03)01368-8.
- [15] J. Allison, et al., Geant4 developments and applications, *IEEE Trans. Nucl. Sci.* 53 (2006) 270–278. doi:10.1109/TNS.2006.869826.
- [16] T. Sato, K. Niita, N. Matsuda, S. Hashimoto, Y. Iwamoto, S. Noda, T. Ogawa, H. Iwase, H. Nakashima, T. Fukahori, K. Okumura, T. Kai, S. Chiba, T. Furuta, L. Sihver, Particle and Heavy Ion Transport code System, PHITS, Version 2.52, *J. Nucl. Sci. Technol.* 50 (2013) 913–923. doi:10.1080/00223131.2013.814553.
- [17] K. Sümmerer, B. Blank, Modified empirical parametrization of fragmentation cross sections, *Phys. Rev. C* 61 (2000) 034607. doi:10.1103/PhysRevC.61.034607.

- [18] K. Sümmerer, Improved empirical parametrization of fragmentation cross sections, *Phys. Rev. C* 86 (2012) 014601. doi:10.1103/PhysRevC.86.014601.
- [19] G. Folger, V. N. Ivanchenko, J. P. Wellisch, The Binary Cascade, *Eur. Phys. J. A* 21 (2004) 407–417. doi:10.1140/epja/i2003-10219-7.
- [20] T. Koi, G. Folger, B. Trieu, J. P. Wellisch, I. Corneliu, P. Truscott, Ion Transport Simulation Using Geant4 Hadronic Physics, Monte Carlo 2005 Topical Meeting ISBN:0-89448-695-0 Chattanooga, Tennessee (April 17-21 2005).
- [21] T. Koi, et al., New native QMD code in Geant4, The Joint International Conference on the 7th Supercomputing in Nuclear Applications and the 3rd Monte Carlo 2010 (SNA+MC2010) (October 17-21 2010).
- [22] K. Niita, S. Chiba, T. Maruyama, T. Maruyama, H. Takada, T. Fukahori, Y. Nakahara, A. Iwamoto, Analysis of the (N,XN') reactions by quantum molecular dynamics plus statistical decay model, *Phys. Rev. C* 52 (1995) 2620–2635. doi:10.1103/PhysRevC.52.2620.
- [23] GEANT4, Available online at <http://geant4.cern.ch/> .
- [24] GEANT4 Physics Reference Manual, Available online at <http://geant4.web.cern.ch/geant4/support/index.shtml> .
- [25] C. Zeitlin, S. Guetersloh, L. Heilbronn, J. Miller, A. Fukumura, Y. Iwata, T. Murakami, Fragmentation cross sections of 290 and 400 MeV/nucleon  $^{12}\text{C}$  beams on elemental targets, *Phys. Rev. C* 76 (2007) 014911. doi:10.1103/PhysRevC.76.014911.



- [26] T. T. Böhlen, F. Cerutti, M. Dosanjh, A. Ferrari, I. Gudowska, A. Mairani, J. M. Quesada, Benchmarking nuclear models of FLUKA and GEANT4 for carbon ion therapy, *Phys. Med. Biol.* 55 (2010) 5833–5847. doi:10.1088/0031-9155/55/19/014.
- [27] B. Alpat, E. Pilicer, S. Blasko, D. Caraffini, F. D. Capua, V. Postolache, G. Saltanocchi, M. Menichelli, L. Desorgher, M. Durante, R. Pleskac, C. L. Tessa, Total and Partial Fragmentation Cross-Section of 500 MeV/nucleon Carbon Ions on Different Target Materials, *Nuclear Science, IEEE Transactions on* 60 (2013) 4673–4682. doi:10.1109/TNS.2013.2284855.
- [28] A. N. Golovchenko, L. Sihver, S. Ota, J. Skvarč, N. Yasuda, S. Kodaira, G. N. Timoshenko, M. Giacomelli, Fragmentation of 370 MeV/n  $^{20}\text{Ne}$  and 470 MeV/n  $^{24}\text{Mg}$  in light targets, *Radiat. Meas.* 45 (2010) 856–860. doi:10.1016/j.radmeas.2010.03.006.
- [29] D. Mancusi, L. Sihver, K. Gustafsson, C. L. Tessa, S. B. Guetersloh, C. J. Zeitlin, J. Miller, L. H. Heilbronn, K. Niita, T. Sato, H. Nakashima, T. Murakami, Y. Iwata, PHITS – benchmark of partial charge-changing cross sections for intermediate-mass systems, *Nucl. Instrum. Meth. B* 254 (2007) 30–38. doi:10.1016/j.nimb.2006.10.070.
- [30] L. Sihver, D. Mancusi, K. Niita, T. Sato, L. Townsend, C. Farmer, L. Pinsky, A. Ferrari, F. Cerutti, I. Gomes, Benchmarking of calculated projectile fragmentation cross-sections using the 3-D, MC codes PHITS, FLUKA, HETC-HEDS, MCNPX\_HI, and NUCFRG2, *Acta Astronautica* 63 (2008) 865–877. doi:10.1016/j.actaastro.2008.02.012.
- [31] S. Jalota, A. Kumar, Comparative study of depth dose-distributions

- and partial fragmentation cross sections of  $^{56}\text{Fe}$  ions on polyethylene using GEANT4, Nucl. Instrum. Meth. B 328 (2014) 8–13. doi:10.1016/j.nimb.2014.02.017.
- [32] A. Ferrari, P. R. Sala, A. Fassò, J. Ranft, FLUKA: a multi-particle transport code, CERN 2005-10 (2005), INFN/TC 05/11, SLAC-R-773 (2005).
- [33] G. Battistoni, S. Muraro, P. Sala, F. Cerutti, A. Ferrari, S. Roesler, A. Fassò, J. Ranft, The FLUKA code: Description and benchmarking, AIP Conf. Proc. 896 (2007) 31–49, Proceedings of the Hadronic Shower Simulation Workshop 2006. doi:10.1063/1.2720455.
- [34] L. H. Khiem, T. Kato, K. Morimoto, M. Notani, A. Ozawa, R. Kanungo, I. Tanihata, A. Yoshida, Production of neutron-rich isotopes by fragmentation of 80 MeV/nucleon  $^{59}\text{Co}$  beam, Nucl. Phys. A 722 (2003) 484c–488c. doi:10.1016/S0375-9474(03)01413-1.
- [35] S. Lukyanov, M. Mocko, L. Andronenko, M. Andronenko, D. Bazin, M. A. Famiano, A. Gade, S. P. Lobastov, W. G. Lynch, A. M. Rogers, O. B. Tarasov, M. B. Tsang, G. Verde, M. S. Wallace, R. G. T. Zegers, Projectile fragmentation of radioactive beams of  $^{68}\text{Ni}$ ,  $^{69}\text{Cu}$ , and  $^{72}\text{Zn}$ , Phys. Rev. C 80 (2009) 014609. doi:10.1103/PhysRevC.80.014609.
- [36] B. Fernández-Domínguez, R. C. Lemmon, B. Blank, M. Chartier, D. Cortina-Gil, J. L. Durell, H. Geissel, J. Gerl, S. Mandal, F. Rejmund, K. Sümmerer, Production cross-sections from neutron-deficient  $^{92}\text{Mo}$  at 500A MeV, Eur. Phys. J. A 25 (2005) 193–198. doi:10.1140/epja/i2005-10104-5.

- [37] EXFOR database, Available online at <http://www.nea.fr/html/dbdata/> .
- [38] P. Napolitani, et al., Measurement of the complete nuclide production and kinetic energies of the system  $^{136}\text{Xe}+\text{hydrogen}$  at 1 GeV per nucleon, *Phys. Rev. C* 76 (2007) 064609. doi:10.1103/PhysRevC.76.064609.
- [39] J. Benlliure, et al., Production of medium-mass neutron-rich nuclei in reactions induced by  $^{136}\text{Xe}$  projectiles at 1 A GeV on a beryllium target, *Phys. Rev. C* 78 (2008) 054605. doi:10.1103/PhysRevC.78.054605.
- [40] J. A. Alcántara-Núñez, et al., Investigating the intra-nuclear cascade process using the reaction  $^{136}\text{Xe}$  on deuterium at 500 A MeV, *EPJ Web of Conferences* 8 (2010) 07012. doi:10.1051/epjconf/20100807012.
- [41] M. Bernas, et al., Fission-residues produced in the spallation reaction  $^{238}\text{U} + \text{p}$  at 1 A GeV, *Nucl. Phys. A* 725 (2003) 213–253. doi:10.1016/S0375-9474(03)01576-8.
- [42] J. Pereira, et al., Isotopic production cross sections and recoil velocities of spallation-fission fragments in the reaction  $^{238}\text{U}(1\text{A GeV}) + \text{d}$ , *Phys. Rev. C* 75 (2007) 014602. doi:10.1103/PhysRevC.75.014602.
- [43] D. Pérez-Loureiro, et al., Production of medium-mass neutron-rich nuclei in  $^{238}\text{U}$  fission, *AIP Conf. Proc.* 1175 (2009) 27–30, Proceedings of 4th International Workshop on Nuclear Fission and Fission-Product Spectroscopy 2009. doi:10.1063/1.3258237.
- [44] K. Sümmerer, W. Brühle, D. J. Morrissey, M. Schädel, B. Szweryn, Y. Weifan, Target fragmentation of Au and Th by 2.6 GeV protons, *Phys. Rev. C* 42 (1990) 2546–2561. doi:10.1103/PhysRevC.42.2546.

- [45] M. Mocko, et al., Projectile fragmentation of  $^{40}\text{Ca}$ ,  $^{48}\text{Ca}$ ,  $^{58}\text{Ni}$ , and  $^{64}\text{Ni}$  at 140 MeV/nucleon, Phys. Rev. C 74 (2006) 054612. doi:10.1103/PhysRevC.74.054612.
- [46] C. Zeitlin, A. Fukumura, S. B. Guetersloh, L. H. Heilbronn, Y. Iwata, J. Miller, T. Murakami, Fragmentation cross sections of  $^{28}\text{Si}$  at beam energies from 290A to 1200A MeV, Nucl. Phys. A 784 (2007) 341–367. doi:10.1016/j.nuclphysa.2006.10.088.
- [47] S. Cecchini, T. Chiarusi, G. Giacomelli, M. Giorgini, A. Kumar, G. Mandrioli, S. Manzoor, A. R. Margiotta, E. Medinaceli, L. Patrizzii, V. Popa, I. E. Qureshi, G. Sirri, M. Spurio, V. Togo, Fragmentation cross sections of  $\text{Fe}^{26+}$ ,  $\text{Si}^{14+}$  and  $\text{C}^{6+}$  ions of 0.3-10 A GeV on polyethylene, CR39 and aluminum targets, Nucl. Phys. A 807 (2008) 206–213. doi:10.1016/j.nuclphysa.2008.03.017.